Terahertz Reflection-Mode Biological Imaging Based on InP HBT Source and Detector

Jongwon Yun, Seung Jae Oh, Kiryong Song, Daekeun Yoon, Hye Young Son, Yuna Choi, Yong-Min Huh, and Jae-Sung Rieh, *Senior Member, IEEE*

***Abstract*—This paper presents the development of an oscillator and a detector based on InP HBT technology operating near 300 GHz, and their application to terahertz reflection-mode imaging. The fabricated fundamental-mode common-base (CB) cross-coupled oscillator exhibits a peak output power of 5.3 dBm at 305.8 GHz, and the CB direct detector shows a responsivity higher than 40 kV/W and noise equivalent power lower than 35 pW/$\sqrt{\text{Hz}}$ for a frequency range of 270–345 GHz. The imaging system employing the fabricated circuits as the signal source and detector was characterized for the resolution and dynamic range, and then, successfully applied for imaging various biological samples. The results show that low-power terahertz reflection-mode imaging based on solid-state electronic sources and detectors based on a commercial semiconductor technology is promising for various biomedical imaging applications.**

***Index Terms*—Detectors, heterojunction bipolar transistors (HBTs), imaging, oscillators, signal generators, terahertz.**

I. Introduction

THE terahertz band, which is located between the traditional microwave and optical spectra, is gaining growing interests from various scientific and engineering communities. One distinctive aspect of this frequency range is the high transparency over a wide variety of nonconducting materials, such as paper, plastics, and fabrics, which are opaque in visible and near-IR regimes. In addition, the terahertz wave shows high reflection and absorption for water-containing materials and is almost fully reflected when radiated at conducting objects such as metal. For this high selectivity over different materials regarding transmission and reflection, the terahertz band has a great potential for various applications, especially for imaging.

When compared to X-rays, which are widely adopted in various imaging systems, terahertz wave involves significantly lower photon energy (4.1 meV at 1 THz); hence, posing little radiation hazards to humans. The vibrational and rotational transition energies of bio-molecules also correspond to the terahertz regime, making it promising for biomedical imaging and spectroscopy applications [1]. In the case of biomedical applications, the differences in water content in bio-samples due to the structural and chemical variations lead to strong contrasts in terahertz imaging. Therefore, various tissues and organs can be differentiated, and deficiencies, such as malignant tumors [2]–[4], burned tissues [5], [6], and dental caries [7], [8], can also be diagnosed by exploiting this unique feature of the terahertz imaging.

One critical component for terahertz imaging systems, especially when commercial applications are considered, is a high-performance signal source. Various types of terahertz signal sources have been deployed for imaging systems. A popular standard approach derived from the terahertz time-domain spectroscopy system uses terahertz pulses generated from femtosecond lasers [9], but the system is rather bulky and hard to bring outside the laboratory environment. Photomixing techniques, including those based on uni-travelling-carrier photodiode [10], [11], have been widely adopted to generate the continuous-wave terahertz wave, but they typically require two separate external laser sources. Solid-state oscillators based on electronic devices are attractive candidates as well, especially when compact and low dc-power consuming sources are desired. Various diode-based oscillators have been successfully deployed, such as Gunn diodes [12], [13], IMPATT (IMPAct ionization Transit Time) diodes [14], [15], and resonance tunneling diodes [16], [17]. However, they are not compatible with regular commercial semiconductor technologies, and thus they are not available for on-chip integration with other electronics parts and are potentially costly. From this perspective, electronic oscillators based on commercial semiconductor technologies best serve the purpose as a compact and power-efficient terahertz signal source, if they provide sufficient operation frequency and output power.

In this paper, a 300-GHz high-power oscillator and a 300-GHz direct detector based on a commercial InP HBT

Manuscript received June 13, 2016; accepted February 6, 2017. Date of publication April 3, 2017; date of current version May 4, 2017. This work was supported by the National Research Foundation of Korea under Grant NRF-2015R1A2A1A05001836 funded by the Korean Government (MEST) *(Jongwon Yun and Seung Jae Oh contributed equally to this work.)*

J. Yun was with the School of Electrical Engineering, Korea University, Seoul 02841, South Korea. He is now with SK Hynix, Gyeonggi 17336, South Korea (e-mail: jwy128@gmail.com).

S. J. Oh and Y. Choi are with the YUHS-KRIBB Medical Convergence Research Institute, Yonsei University College of Medicine, Seoul 03722, South Korea (e-mail: issac@yuhs.ac; gksmf589@naver.com).

H. Y. Son is with the Severance Biomedical Science Institute, Severance Hospital, Yonsei University College of Medicine, Seoul 03722, South Korea (e-mail: shy916@yuhs.ac).

Y.-M. Huh is with the YUHS-KRIBB Medical Convergence Research Institute, Yonsei University College of Medicine, Seoul 03722, South Korea, and also with the Department of Radiology, Severance Hospital, Yonsei University College of Medicine, Seoul 03722, South Korea (e-mail: ymhuh@yuhs.ac).

K. Song and J.-S. Rieh are with the School of Electrical Engineering, Korea University, Seoul 02841, South Korea (e-mail: acoor@korea.ac.kr; jsrieh@korea.ac.kr).

D. Yoon was with the School of Electrical Engineering, Korea University, Seoul 02841, South Korea. He is now with the International College of Semiconductor and Technology, National Chiao Tung University, Hsinchu 300, Taiwan (e-mail: dkyoon99@gmail.com).

Color versions of one or more of the figures in this paper are available online at http://ieeexplore.ieee.org.

Digital Object Identifier 10.1109/TTHZ.2017.2673549

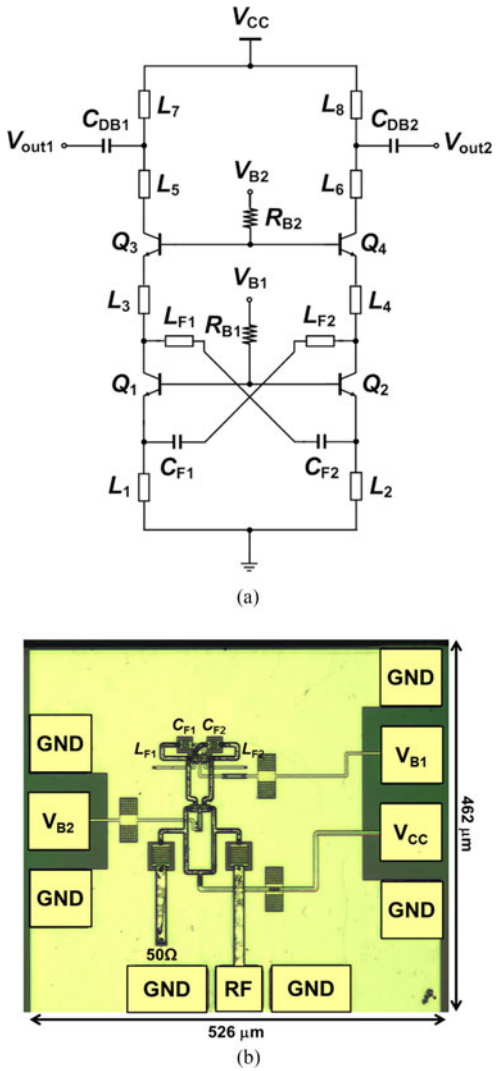

Fig. 1. (a) Schematic and (b) chip photograph of the developed 300-GHz fundamental-mode oscillator.

technology were developed and employed for terahertz imaging. With the transistor-based source and detector, terahertz reflection imaging was carried out for various biological tissues. In this way, the potential of the developed imaging system for biomedical applications has been explored, which is the main purpose of this paper.

II. Signal Source and Detector

A. Signal Source

The schematic and the chip photograph of the signal source used for imaging in this paper is shown in Fig. 1(a) and (b), respectively. It is basically a 300-GHz high-power oscillator, and the details were reported in [18]. The key perspectives are provided here for the sake of convenience. The oscillator is based on an *LC* cross-coupled topology, and employs the common-base (CB) cross-coupled structure rather than the conventional common-emitter (CE) cross-coupled structure. Compared to the CE cross-coupled topology, the CB cross-coupled configuration is known to exhibit a negative conductance at higher frequencies, resulting in higher oscillation frequencies [18]. As the

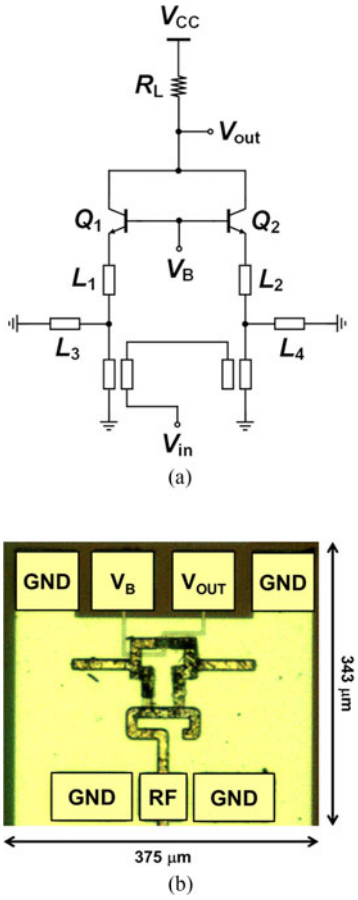

Fig. 2. (a) Schematic and (b) chip photograph of the fabricated 300-GHz direct detector.

output buffer, a CB amplifier stage is adopted, which is stacked over the oscillator core. Generally, CB amplifiers show a higher maximum available gain compared to CE amplifiers in the terahertz band, and are consequently expected to further boost the intensity of the oscillation signal when used as a buffer. The output is taken in a differential manner, where one output node is 50 Ω terminated and the other node leads to a probe pad to enable single-ended on-wafer probing.

The oscillator was fabricated in Teledyne's 250-nm InP HBT technology [19]. The measured oscillation frequency is 305.8 GHz and the phase noise is −116.5 dBc/Hz at 10-MHz offset. The measured output power is 5.3 dBm after calibration, for which a loss of 6.5 dB from the RF probe and waveguides was compensated. The corresponding dc-power dissipation is 87.4 mW, leading to a dc-to-RF efficiency of 3.9%.

B. Detector

Fig. 2(a) and (b) display the schematic and die photograph of the 300-GHz direct detector, respectively. The detector is basically a square-law detector, which exploits the nonlinearity of the transistor to convert the input RF signals into dc output voltage signals that are proportional to the input power [20]. Due to the device nonlinearity, harmonic components will be generated at the output current (collector current), and the even harmonics, including the dc component, will add up, while the odd harmonics cancel out at the collector common node of

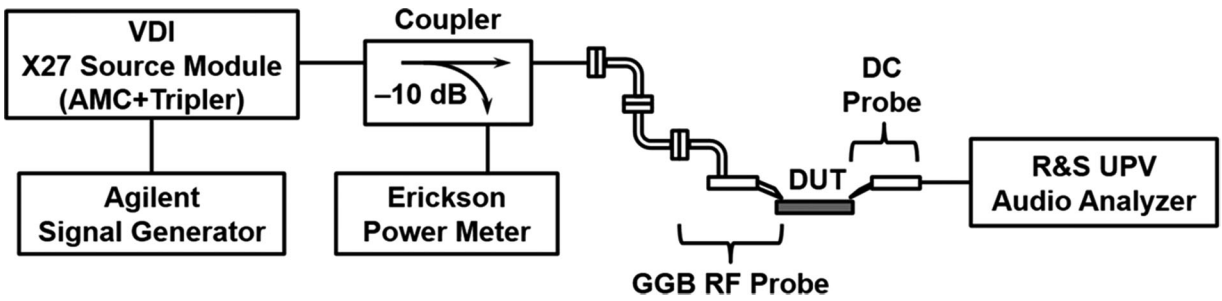

Fig. 3. Measurement setup for electrical characterization of the detector.

the differential pair. In this paper, a differential pair based on the CB topology is adopted for the direct detector, where the differential RF signals are injected through the emitters of the core transistors. It is known that the CB topology shows a larger responsivity and lower noise level, especially at high frequency bands, and also exhibits wider bandwidth characteristics than the CE topology [21]. The emitters are conjugate-matched to the input of the detector at 300 GHz with series transmission lines and stubs for maximum power delivery in the direct detection. To enable a single-ended injection, a 300-GHz Marchand balun is employed at the input, which is implemented with stacked coupled lines composed of two top metal layers. The output is taken from the collector common node of the differential pair to extract the output signal, in which a 5.6-kΩ resistor is used as a load as well as an RF choke.

The direct detector was fabricated in Teledyne's 250-nm InP HBT technology. The measurement setup used to characterize its electrical properties is shown in Fig. 3. A 250–375-GHz signal source module composed of a VDI WR9.0 AMC and a WR2.8 frequency tripler (total multiplication factor of 27) driven by a signal generator was used for the generation of the input signal. An attenuator included in the source module was used to enable the power level adjustment. An audio signal analyzer was used to measure the responsivity and noise equivalent power (NEP). The input signal was amplitude-modulated to suppress the flicker noise, while the input power was monitored by a power meter coupled by a -10-dB directional coupler. The measured characteristics are shown in Fig. 4. The detector exhibits a wide bandwidth of roughly 270–345 GHz with responsivity higher than 40 kV/W and NEP lower than 35 pW/$\sqrt{\text{Hz}}$. The maximum responsivity and minimum NEP are 55.9 kV/W and 25.6 pW/$\sqrt{\text{Hz}}$, respectively. It is noted that the measured responsivity is much larger than the detectors with a similar topology based on SiGe HBT [20] or Si CMOS [22], [23] technologies, while the NEP falls on a similar level as those Si-based detectors. Since the detector operates with low dc bias conditions to enhance the square-law detection efficiency, the power dissipation is only 0.17 mW.

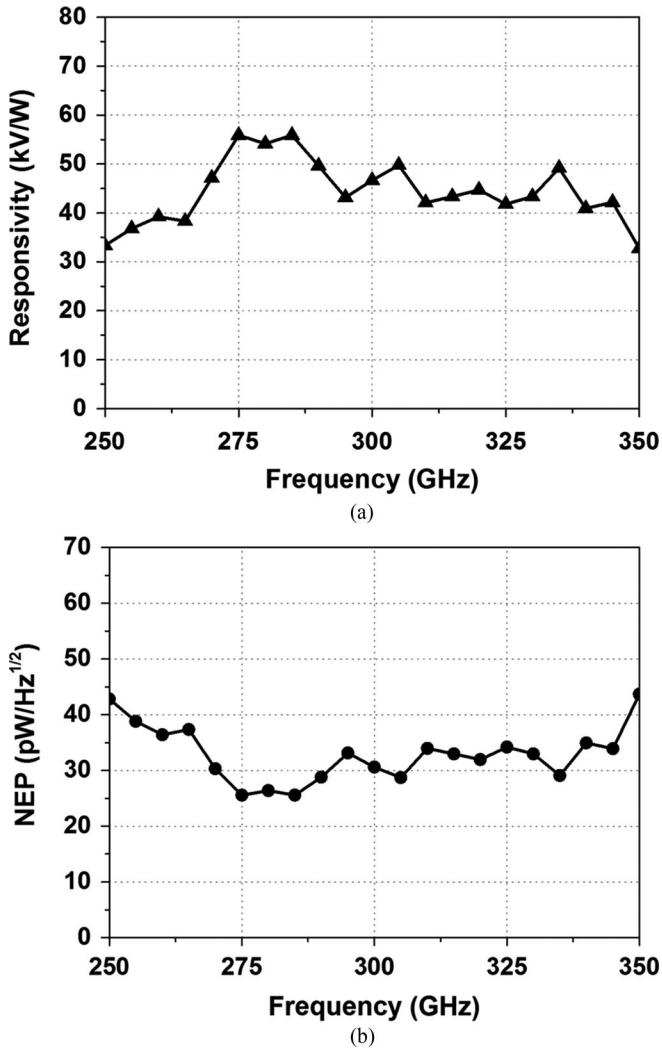

Fig. 4. Measurement results of the direct detector: (a) Measured responsivity and (b) measured NEP.

III. Reflection-Mode Imaging Setup

A. Imaging Setup

One of the unique characteristics of the terahertz wave is its highly selective property, both in transmission and reflection, against different water content levels of the target materials. This can be exploited for biomedical imaging applications, since water constitutes a large fraction of biological samples and the water content level varies depending on the structural and chemical properties of the sample. Hence, a strong contrast is expected to be obtained over different samples, as well as over different parts of a given sample, if the water content varies. While such selective property can be used for both

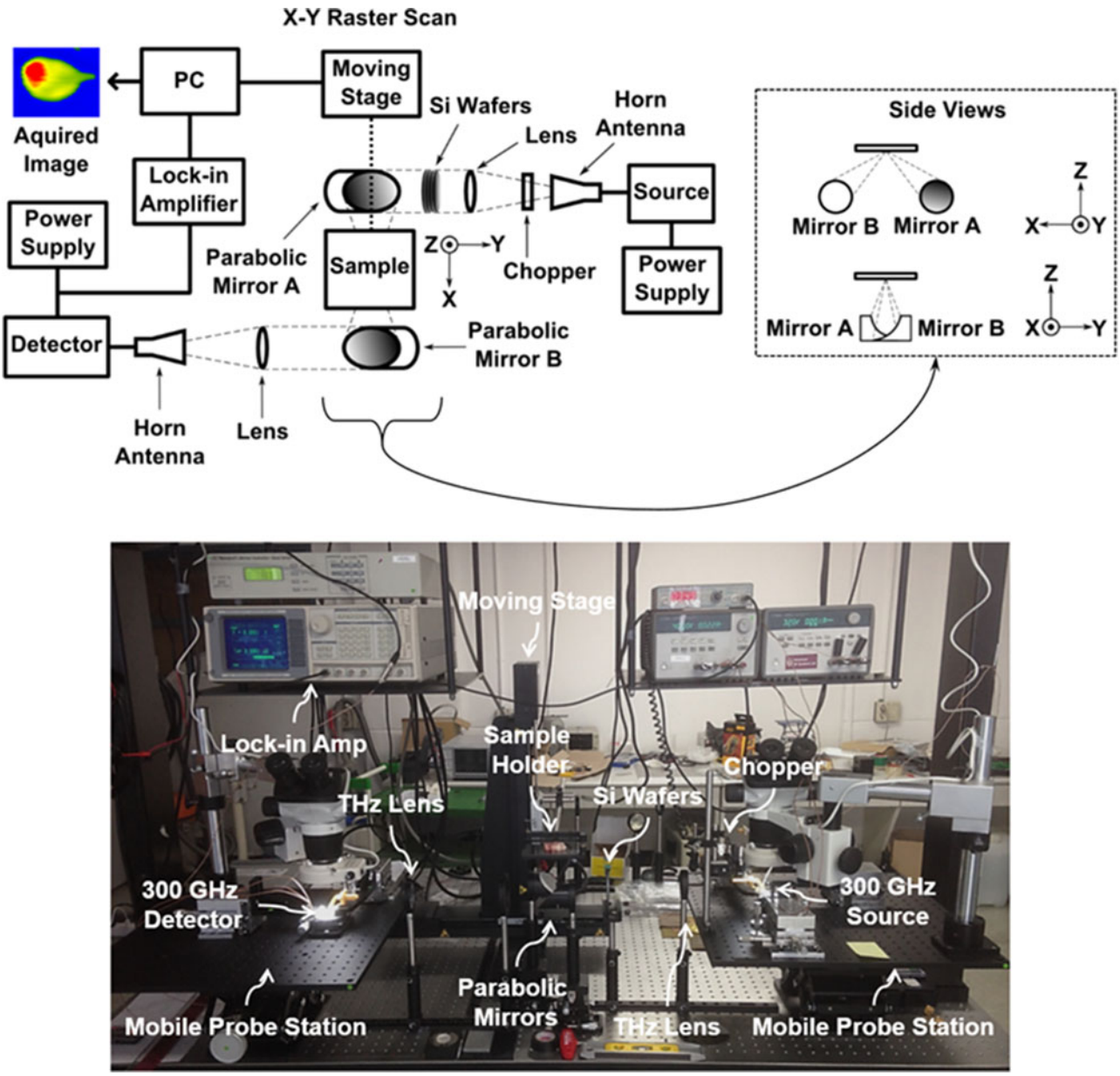

Fig. 5. Reflection-mode terahertz imaging setup (top: block diagram, bottom: photograph).

transmission and reflection imaging, the transmission imaging requires the target biological sample to be very thin, because of the strong absorption by the water inside the sample. This severely limits the transmission-mode imaging of biological subjects, virtually preventing *in vivo* applications. On the other hand, the reflection-mode imaging does not suffer from this limit, making it a more preferred modality in terahertz imaging for biomedical applications.

In order to examine the practical applicability of the developed circuits for the reflection-mode imaging, a series of experiments were carried out with the fabricated oscillator and detector. The reflection-mode imaging setup developed in this paper is illustrated in Fig. 5, which adopts the oscillator and the detector as the signal source and the image detector, respectively. Imaging experiments are carried out while the source and detector chips are on-wafer probed. For this, two mobile probe stations are built on top of X-Y-Z stages, so that their position can be adjusted independently. This enables the optical alignment between the components in the setup while the chips remain on-wafer probed. Horn antennas are connected to the source and detector chips through RF probes (GGB WR3.4 probes) to transmit and receive the terahertz signals.

Terahertz lenses and off-axis parabolic mirrors are adopted to guide and focus the terahertz signal. The focal length of the terahertz lens is 100 mm and the effective and parent focal length of the off-axis parabolic mirrors are 101.6 and 50.8 mm, respectively. The clear aperture of the parabolic mirrors is 45.7 mm (90% of the mirror diameter of 50.8 mm), and the incidence angle with respect to the target normal is 23.5°. The standoff distance between the mirror and the top surface of the quartz crystal is 101.6 mm. Located at the center of the setup is a

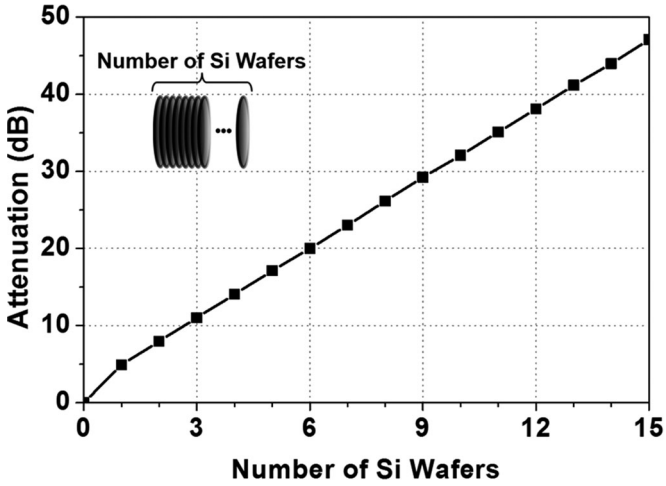

Fig. 6. Attenuation level for various number of Si wafers placed side-by-side.

sample holder that is driven by a moving stage for a 2-D raster scan. A quartz glass with a thickness of 3 mm is fixed at the bottom of the sample holder, the thickness being chosen to minimize the reflection of the 300-GHz signal from the glass itself. The output of the detector is connected to a lock-in amplifier, where the signal intensity is quantified and transferred to a PC for image reconstruction. In addition, a chopper is employed right after the horn antenna of the signal source to mechanically modulate the terahertz signal at a frequency of 350 Hz. In addition, a set of Si wafers are placed (in contact with each other) between the lens and parabolic mirror on the signal source-side as a means to control the signal power reaching the sample. Fig. 6 shows the attenuation level of the Si wafers as a function of the number of wafers, indicating the effective attenuation obtained by the Si wafers. Each wafer contributes roughly 3 dB of attenuation, while there is an additional ∼3-dB loss from the first wafer, which is assumed to be caused by the initial reflection. An attenuation as large as 48 dB was obtained with 15 wafers, which is much larger than the typical maximum attenuation level of 30 dB available from commercial attenuators at this frequency range. Hence, this method provides a much wide range of attenuation with a simple configuration.

B. *Characterization of the Setup*

Prior to imaging the target objects, the imaging setup was first characterized in terms of dynamic range and resolution, which would directly affect the quality of the acquired images. The dynamic range was estimated as the ratio between the maximum signal (i.e., full reflection) and the noise level measured at the detector side. The maximum signal was measured by the lock-in amplifier with an aluminum plate placed on the sample holder, assuming it fully reflects the terahertz signal from the signal source. The noise level was measured with the source signal fully blocked by placing the same plate between the lens and parabolic mirror. For reliable data, the measurement was repeated 50 times and averaged. Since the measured noise level is in the unit of V/$\sqrt{\text{Hz}}$, the square-root of the equivalent noise bandwidth, which was 1.1 $\sqrt{\text{Hz}}$ at the time of measurement,

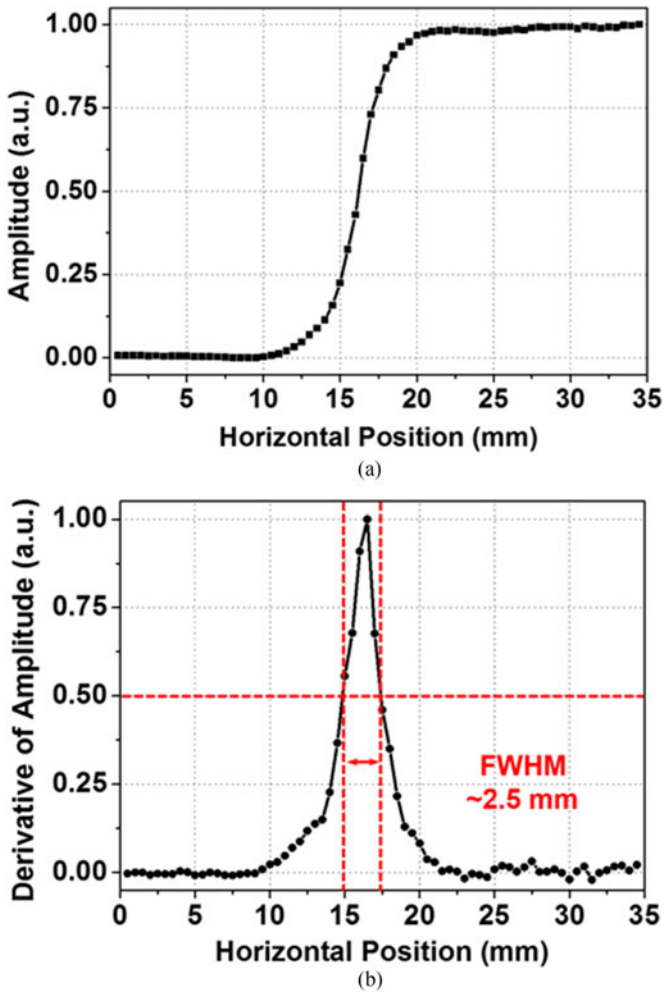

Fig. 7. Measured resolution of the reflection-mode terahertz imaging setup: (a) Edge response and (b) line spread function (FWHM around 2.5 mm).

was multiplied to the measured value to obtain the noise voltage level. The average values of the maximum signal and the noise level were 0.8 V and 3.2 μV, respectively, leading to a voltage dynamic range of 107.9 dB. It is noted that for the actual imaging setup, the sample is placed on top of a quartz glass as a means to hold the sample at the beam target point. Hence, even without the presence of a sample, the quartz glass remains at the location, partially reflecting the signal. If we should consider this inevitable reflection from the quartz glass, the actual dynamic range will be significantly lower than this value. Based on the data used for Fig. 7, this "effective dynamic range" of the imaging setup is estimated to be 36.7 dB.

To investigate the resolution of the 300-GHz reflection-mode setup, the edge response and the line spread function were obtained by measuring the signal reflected from a sharp metal razor that was placed on the quartz glass. The results are shown in Fig. 7, which were obtained with a 500-μm scanning step. The signal amplitude and its derivative were normalized into 0 to 1 scale in the plot. The line spread function, which represents the profile of the corresponding Gaussian beam, can be attained by finding the derivative of the edge response. The full width of the line spread function at half its maximum value (FWHM) can be considered as the resolution of a specific imaging

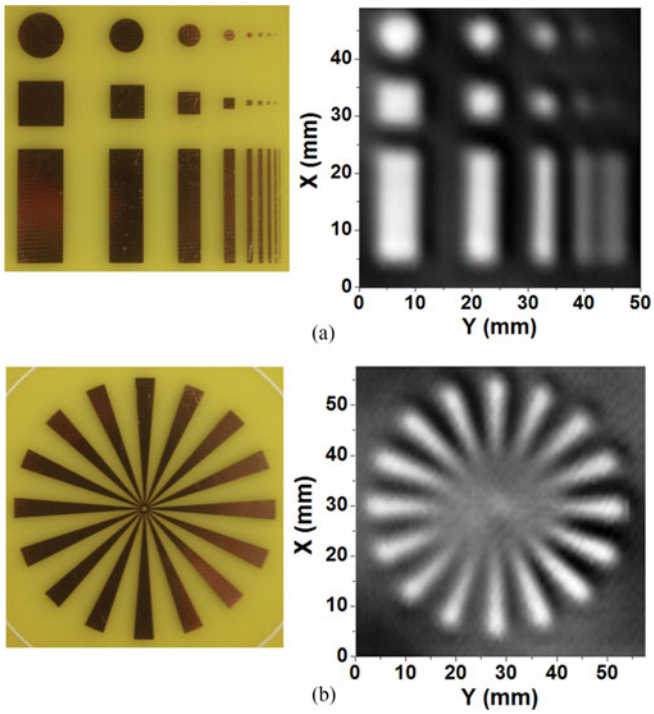

Fig. 8. Visible images (left) and the acquired images (right) of resolution patterns. (a) Circles, squares, rectangles. (b) Sunflower.

system [24]. The measured FWHM indicates that the resolution of the reflection-mode terahertz imaging system is around 2.5 mm. This is consistent with the estimated value of 2.1 mm, which can be calculated based on the beam diameter at the horn antenna radiation point and the focal lengths of the lens and the mirror employed.

For a visual inspection of the resolution, metal resolution patterns drawn on PCB boards were imaged with the imaging setup. Fig. 8 shows the visible images (left) and the acquired images (right) of the patterns that were scanned with a step size of 500 μm. The images of both patterns show that the shapes become fuzzy as the width decreases roughly below 2 mm. The result is consistent with the obtained FWHM of 2.5 mm.

IV. Terahertz Imaging on Biological Samples

Based on the imaging setup described above, reflection imaging was carried out for various biological samples. For the imaging experiments, following circuit bias conditions were used: $V_{\rm CC} = 4$ V, $V_{\rm B2} = 3.3$ V, $V_{\rm B1} = 1.3$ V for the oscillator; $V_{\rm CC} = 3$ V, $V_B = 0.68$ V for the detector. With this bias condition, the source frequency was fixed at 305.8 GHz and no frequency modulation was employed. The corresponding total dc power needed to drive the source and the detector was only 87.6 mW.

A. Internal Organ Tissues of a Mouse

To compare the reflection properties of various biological tissues for the terahertz signal generated, internal organs of a mouse, including muscle, spleen, kidney, brain, and liver, were imaged. The fresh organ tissues were extracted surgically after euthanasia from 5–8-week-old male BALB/c-nude mice. All

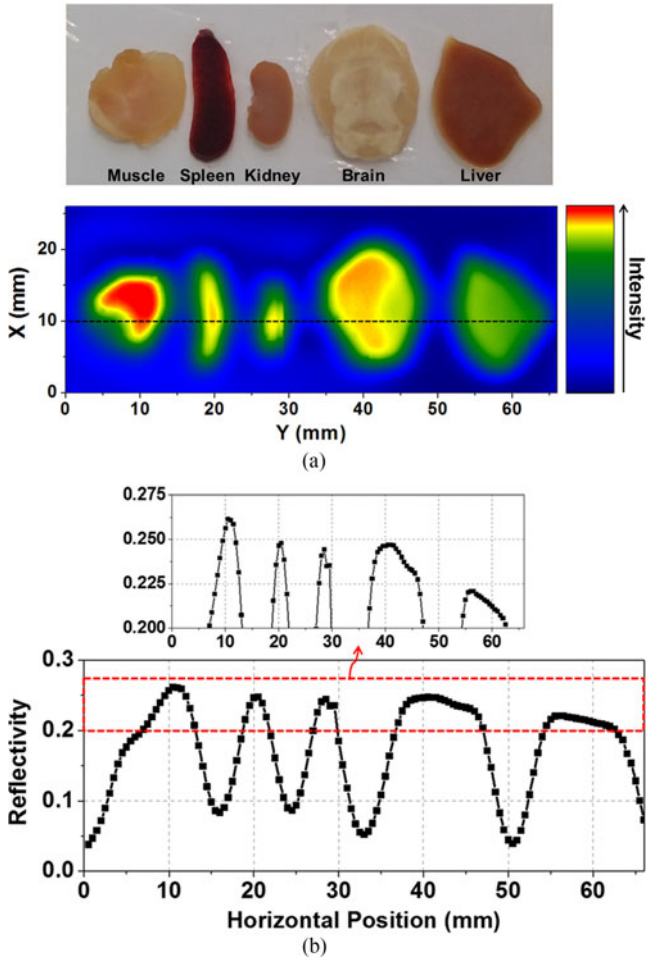

Fig. 9. *Ex vivo* imaging results of the internal organs of a mouse. (a) Visible (up) and acquired image (down). (b) Reflectivity along the reference line.

animal experiments were conducted with the approval of the Institutional Animal Care and Use Committee, Yonsei University Health System. The organs were placed on top of the 3-mm thick quartz glass and fixed to the sample holder of the imaging setup.

Ex vivo imaging results for the internal organs of a mouse are shown in Fig. 9, where the visible and acquired images are displayed in Fig. 9(a) and the reflectivity across the horizontal dotted reference line is presented in Fig. 9(b). The reflectivity is defined as the ratio between the reflected and incident signal (maximum signal reflection from metal plate) amplitude. The color scale was chosen in a way to maximize the contrast in the image for each case. As shown in the acquired image, the shapes of the internal organs are clearly visible, while subtle differences in the reflectivity between the tissues are also observed. The dotted region in the plot is magnified in a separate plot for a more precise comparison of the reflectivity.

The differences in the reflectivity between the organs clearly indicate the different water content level in each organ. It is noted that the dehydration of biological samples during the sample preparation and imaging acquisition may screen the true water content of the sample, especially when the sample volume is small. For the imaging with a single pixel detector that requires

raster scanning, as is the case for this paper, the increase in the scan step size may reduce the time for image acquisition, which leads to a tradeoff with the image resolution. It took $\sim$40 min for the image shown in Fig. 9 with a scan step size of 500 μm.

To investigate the effect of signal source power on the imaging of biological samples, the source power incident on the sample was varied. The attenuation with Si wafers, as described earlier, was used for the incident power control. For this experiment, the scan step size was increased to 1 mm, in order to reduce the overall scanning time. Other conditions for the source and detector remained unchanged.

Fig. 10 shows the imaging results of the same set of organs with varied incident power. The corresponding reflectivity profiles along the reference lines are also presented. Fig. 10(a)–(d), respectively, show the results with following attenuation: 9, 18, 27, and 36 dB. The images were taken in the order from lower to higher attenuation and each imaging took around 10 min for acquisition. Roughly, 2 min was taken to adjust the attenuation level by inserting extra Si wafers. It is expected that dehydration during the imaging was not excessive with the sample thickness of over 2 mm, especially when the imaged surfaces of the organs were firmly attached to the quartz glass and covered by plastic wrap. It is observed from the acquired images that the differences between the organs are clear even with the attenuation up to 18 dB. The profiles of the reflectivity along the reference lines are also similar to those without attenuation. The images begin to degrade with the attenuation of 27 dB, and the differences in the reflectivity between the organs can hardly be seen when the attenuation reaches 36 dB. The sample boundary is also distorted with 36-dB attenuation, although the presence of the sample is still clear from the image. The results indicate that the developed reflection imaging system provides useful information on biological samples even with quite small source power. It is noted that there is a slight fluctuation in the peak reflectivity levels over the plots. This may be ascribed to the fact that a fixed power level from the signal source was assumed for the calculation of the reflectivity in the plots, while the actual signal source power might have been different for each plot. Relatively more stabilized signal sources based on locking techniques, such as injection-locked sources or phase-locked loops, are expected to effectively suppress the drift in the signal source output power.

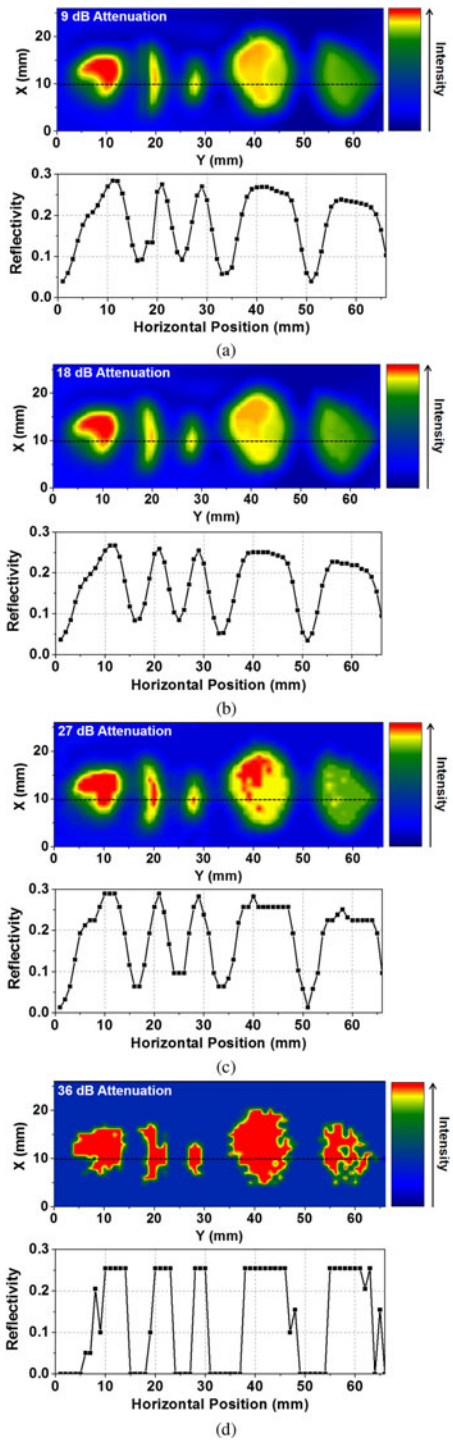

Fig. 10. Acquired images and reflectivity along the reference line for internal organs with source power varied. (a) 9-dB, (b) 18-dB, (c) 27-dB, and (d) 36-dB attenuation.

B. Brain Tumor of a Rat

To explore the possibility of applying the reflection imaging system to cancer studies, a brain tissue of a rat with a tumor was imaged. The cerebral tumor animal model is based on an orthotopic glioma model of a rat. 9L/lacZ rat glioma cells were surgically implanted into a nine-week-old male Sprague–Dawley rat, and a T2-weighted MRI was used to monitor the growth of the tumor for 3–4 weeks. The brain tissue was obtained surgically after euthanasia when the cancer size grew over 1 cm^3. The brain was divided into two sides, side A and B, at the transverse plane with a surgical knife. Fig. 11 shows the *ex vivo* imaging results of the brain tissues with the tumor. The visible (left) and acquired (right) images and the reflectivity profile along the reference line of side A are displayed in Fig. 11(a) and (b), respectively. Those of side B are shown in Fig. 11(c) and (d). Both tissues were scanned with a step size of 500 μm. The bias conditions for the oscillator and detector were the same as described earlier.

The acquired images clearly display the shapes of the brain tissues and, more importantly, the cancerous regions with high contrast, which well matches the tumor sections shown in the

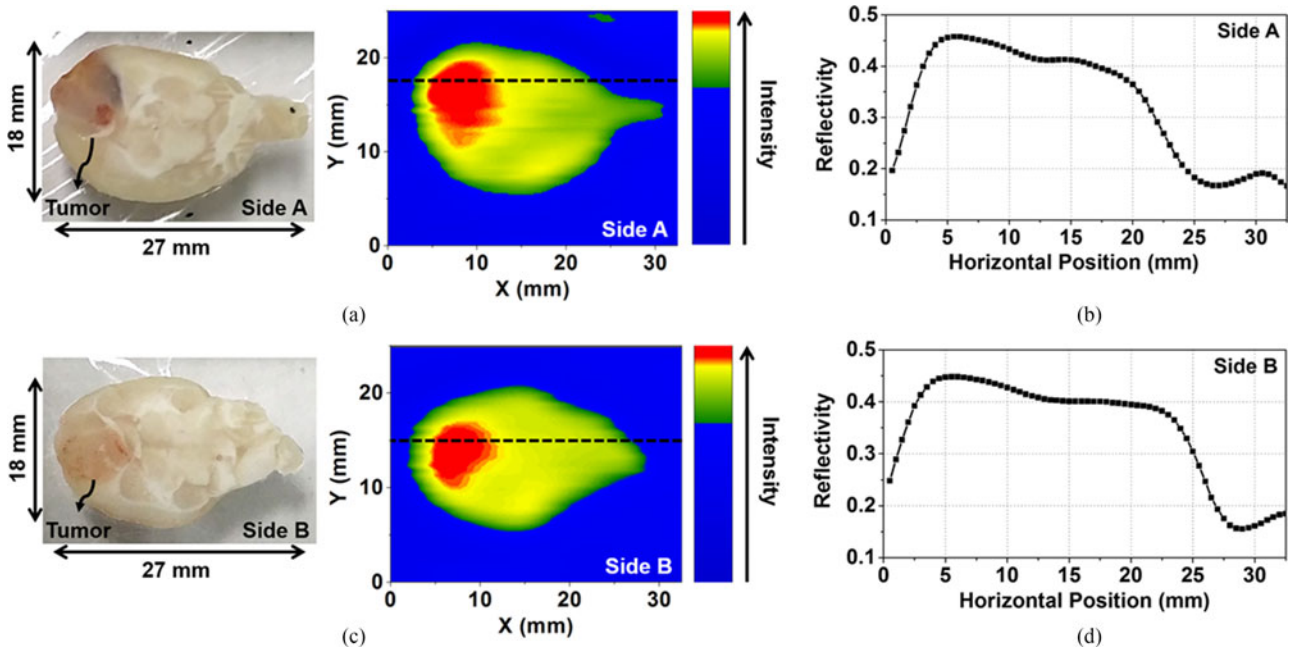

Fig. 11. *Ex vivo* imaging results of the brain tissue of a rat with a tumor. (a) Visible (left) and acquired image (right) of side A. (b) Reflectivity of side A along the reference line. (c) Visible (left) and acquired image (right) of side B. (d) Reflectivity of side B along the reference line.

visible images. The obtained reflectivity from the tumor areas are clearly higher than those from the normal regions, indicating the higher water content in cerebral tumor. The higher water content arises from various biological reactions, such as body fluid around the necrotic debris and newly generated blood vessels [2]. The reflectivity characteristics of both brain tissues are similar, where the cancerous regions exhibit the reflectivity of 45%–46% and the normal sections show that of 40%–41%, leading to a difference of 5%. This difference is expected to be sufficient to highlight the cancerous region against the normal region. Although the experiment was performed as *ex vivo* imaging, it can be extended to *in vivo* imaging in principle, which is a major advantage of the reflection-mode over the transmission-mode imaging. To be adopted for *in vivo* imaging applications, the setup needs to become more compact so that it can be a table-top tool or, more preferably, a hand-held tool, which can be conveniently used for *in vivo* studies of the surface of a human body, such as skin, tooth, and so forth. In addition, the nonionizing nature of the terahertz wave would make it a highly preferred modality from a health hazard point of view. One limitation is that the penetration depth of the terahertz wave is only about 0.2 mm near 300 GHz [25] and, thus, only tumors exposed on the surface or located very close to the surface can be detected with the terahertz reflection imaging. When compared to other results obtained with pulse-based imaging setup [2], [3], the images acquired in this paper show consistent results that highlight the higher water content in cancerous regions. This indicates that the transistor-based imaging system, which benefits from the compact size, low cost, and low power dissipation, can be considered as an alternative for the currently dominating optics-based imaging systems.

V. Conclusion

In this work, an oscillator and a detector operating near 300 GHz were developed based on a commercial InP HBT technology and successfully applied for terahertz imaging. With the reflection-mode imaging system developed employing the fabricated oscillator and detector, various biological samples, including a brain with a tumor were imaged. The imaging results prove that the fabricated oscillator and detector are promising candidates for various biomedical applications with small dc power dissipation and form factor. When combined with integrated on-chip antennas and compact optical components such as Si lenses, they will surely pave a way towards compact and mobile terahertz imaging systems.

References

[1] P. H. Siegel, "Terahertz technology in biology and medicine," *IEEE Trans. Microw. Theory Techn.*, vol. 52, no. 10, pp. 2438–2447, Oct. 2004.
[2] S. J. Oh *et al.*, "Study of freshly excised brain tissues using terahertz imaging," *Biomed. Opt. Exp.*, vol. 5, no. 8, pp. 2837–2842, Jul. 2014.
[3] J. Y. Park, H. J. Choi, G.-E. Nam, K.-S. Cho, and J.-H. Son, "In vivo dual-modality terahertz/magnetic resonance imaging using superparamagnetic iron oxide nanoparticles as a dual contrast agent," *IEEE Trans. Terahertz Sci. Technol.*, vol. 2, no. 1, pp. 93–98, Jan. 2012.
[4] K. Ajito and Y. Ueno, "THz chemical imaging for biological applications," *IEEE Trans. Terahertz Sci. Technol.*, vol. 1, no. 1, pp. 293–300, Sep. 2011.
[5] D. M. Mittleman *et al.*, "Recent advances in terahertz imaging," *Appl. Phys. B, Photophys. Laser Chem.*, vol. B68, no. 6, pp. 1085–1094, Jun. 1999.
[6] S. M. Kim and P. Kung, "Terahertz functional tissue imaging," in *Proc. Prog. Electromagn. Res. Symp.*, 2013, pp. 434–437.
[7] D. Crawley *et al.*, "Three-dimensional terahertz pulse imaging of dental tissue," *J. Biomed. Opt.*, vol. 8, no. 2, pp. 303–307, Apr. 2003.
[8] D. A. Crawley *et al.*, "Terahertz pulse imaging: A pilot study of potential applications in dentistry," *Caries Res.*, vol. 37, no. 5, pp. 352–359, Sep.–Oct. 2003.

[9] Q. Wu, T. D. Hewitt, and X. C. Zhang, "Two-dimensional electro-optic imaging of THz beams," *Appl. Phys. Lett.*, vol. 69, no. 8, pp. 1026–1028, Aug. 1996.
[10] H.-J. Song *et al.*, "Uni-travelling-carrier photodiode module generating 300 GHz power greater than 1 mW," *IEEE Microw. Wireless Compon. Lett.*, vol. 22, no. 7, pp. 363–365, Jul. 2012.
[11] G. Ducournau *et al.*, "Ultrawide-bandwidth single-channel 0.4-THz wireless link combining broadband quasi-optic photomixer and coherent detection," *IEEE Trans. Terahertz Sci. Technol.*, vol. 4, no. 3, pp. 328–337, May 2014.
[12] H. Eisele, "480 GHz oscillator with an InP Gunn device," *Electron. Lett.*, vol. 46, no. 6, pp. 422–423, Mar. 2010.
[13] Y. Wang, L.-A. Yang, W. Mao, S. Long, and Y. Hao, "Modulation of multidomain in AlGaN/GaN HEMT-like planar Gunn diode," *IEEE Trans. Electron. Devices*, vol. 60, no. 5, pp. 1600–1606, May 2013.
[14] M. Ino, T. Ishibashi, and M. Ohmori, "C.W. oscillation with p+–p–n+ silicon IMPATT diodes in 200 GHz and 300 GHz bands," *Electron. Lett.*, vol. 12, no. 6, pp. 148–149, Mar. 1976.
[15] M. Mukherjee, N. Mazumder, and S. K. Roy, "Photosensitivity analysis of gallium nitride and silicon carbide terahertz IMPATT oscillators: Comparison of theoretical reliability and study on experimental feasibility," *IEEE Trans. Device Mater. Rel.*, vol. 8, no. 3, pp. 608–620, Sep. 2008.
[16] M. Asada, S. Suzuki, and N. Kishimoto, "Resonant tunneling diodes for sub-tarahertz and terahertz oscillators," *Jpn. J. Appl. Phys.*, vol. 47, no. 6, pp. 4375–4384, Jun. 2008.
[17] K. Okada, K. Kasagi, N. Oshima, S. Suzuki, and M. Asada, "Resonant-tunneling-diode terahertz oscillator using patch antenna integrated on slot resonator for power radiation," *IEEE Trans. Terahertz Sci. Technol.*, vol. 5, no. 4, pp. 613–618, Jul. 2015.
[18] J. Yun, D. Yoon, H. Kim, and J.-S. Rieh, "300-GHz InP HBT oscillators based on common-base cross-coupled topology," *IEEE Trans. Microw. Theory Techn.*, vol. 62, no. 12, pp. 3053–3064, Dec. 2014.
[19] M. Rodwell *et al.*, "Frequency Limits of InP-based integrated circuits," in *Proc. IEEE Int. Conf. Indium Phosphide Related Mater.*, 2007, pp. 9–13.
[20] D. Yoon, M. Kaynak, B. Tillack, and J.-S. Rieh, "A wideband H-band image detector based on SiGe HBT technology," *J. Electromagn. Eng. Sci.*, vol. 14, no. 1, pp. 59–61, Jan. 2015.
[21] D. Yoon *et al.*, "A D-band active imager in a SiGe HBT technology," *J. Infrared, Millimeter, Terahertz Waves*, vol. 36, no. 4, pp. 335–349, Apr. 2015.
[22] M. Uzunkol *et al.*, "Millimeter-wave and terahertz sources and imaging systems based on 45 nm CMOS technology," *in IEEE MTT-S Int. Microw. Symp. Dig.*, 2012, pp. 1–3.
[23] F. Schuster *et al.*, "Broadband terahertz imaging with highly sensitive silicon CMOS detectors," *Opt. Exp.*, vol. 19, no. 8, pp. 7827–7832, 2011
[24] T. Knopp, S. Biederer, T. F. Sattel, M. Erbe, and T. M. Buzug, "Prediction of the spatial resolution of magnetic particle imaging using the modulation transfer function of the imaging process," *IEEE Trans. Med. Imag.*, vol. 30, no. 6, pp. 1284–1292, Jun. 2011.
[25] O. P. Gandhi and A. Riazi, "Absorption of millimeter waves by human beings and its biological implications," *IEEE Trans. Microw. Theory Techn.*, vol. 34, no. 2, pp. 228–235, Feb. 1986.

Jongwon Yun received the B.S. and Ph.D. degrees in electrical engineering from Korea University, Seoul, South Korea, in 2007 and 2015, respectively. His doctoral dissertation involved the development of signal sources for millimeter-wave and terahertz applications.

In 2015, he was a Research Professor with the School of Electrical Engineering, Korea University, and in 2016, he joined the SK Hynix Research and Development Division, Gyeonggi, South Korea, where he is currently a Senior Research Engineer. His primary research interests include millimeter-wave and terahertz integrated circuits and transceiver systems for imaging and broadband communication applications.

Dr. Yun was the recipient of the Best Student Paper Award of the IEEE Radio Frequency Integration Technology Symposium in 2015.

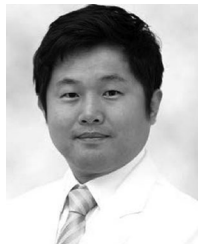

Seung Jae Oh received the B.S., M.S., and Ph.D. degrees in physics from the University of Seoul, Seoul, South Korea, in 2000, 2002, and 2007, respectively.

He was a Postdoctoral Research Fellow with the College of Medicine, Yonsei University, from 2007 to 2009. In 2009, he was a Research Fellow with the Department of Radiology, Yonsei University. Since 2010, he has been a Research Assistant Professor with the YUHS-KRIBB Medical Convergence Research Institute, Yonsei University. His research interests include the area of biomedical optics imaging that includes terahertz wave imaging and ultrafast laser biomedical application.

Kiryong Song received the B.S. degree in electronic engineering from Korea University, Seoul, South Korea, in 2012, where he is currently working toward the Ph.D. degree at the School of Electrical Engineering.

His major research interests include the design of Si-based millimeter-wave oscillators, mixers, and detectors for high-speed wireless communication and imaging systems.

Daekeun Yoon received the B.S. and Ph.D. degrees from the School of Electrical Engineering, Korea University, Seoul, South Korea, in 2006 and 2015, respectively.

From March 2015 to January 2016, he was a Research Professor with Korea University, where he was involved in the design and characterization terahertz 3-D tomographic imaging system. In 2016, he joined the faculty of the International College of Semiconductor and Technology, National Chiao Tung University, Hsinchu, Taiwan. His research interests include millimeter-wave and terahertz integrated circuits for imaging and transceiver systems.

Hye Young Son received the integrated M.A./Ph.D. degree in philosophy in agricultural biotechnology from Seoul National University, Seoul, South Korea, in 2009.

From 2010 to 2014, she was a Director's Postdoctoral Fellow with the Department of Radiology, College of Medicine, Yonsei Univeristy, Seoul, South Korea, where she has been a Research Assistant Professor since 2014. Her research interests are focused on nanomedical imaging with theranosis and stem cell research.

Yuna Choi received the integrated B.S. degree in agricultural science from Korea National Open University, Seoul, South Korea, in 2013.

Since 2011, she has been a Researcher with the Department of Radiology, College of Medicine, Yonsei Univeristy, Seoul, South Korea. Her research interests include the animal modeling and nanomedical imaging with theranosis.

Yong-Min Huh received the M.D. and Ph.D. degrees from the College of Medicine, Yonsei Univeristy, Seoul, South Korea, in 1994 and 2005, respectively.

In 2005, he started an independent research career as an Assistant Professor with the Department of Radiology, College of Medicine, Yonsei University, where he has been a Professor since 2014. His main research interests include the development of translational research, trying to make a bridge between nanoscience and clinical applications.

Jae-Sung Rieh (S'89–M'91–SM'05) received the B.S. and M.S. degrees in electronics engineering from Seoul National University, Seoul, South Korea, in 1991 and 1995, respectively, and the Ph.D. degree in electrical engineering from the University of Michigan, Ann Arbor, MI, USA, in 1999.

In 1999, he joined the IBM Semiconductor Research and Development Center, where he was responsible for the research and development activities for high-frequency SiGe HBT technologies. Since 2004, he has been with the School of Electrical Engineering, Korea University, Seoul, South Korea, where he is currently a Professor. In 2012, he was with the Submillimeter Wave Advanced Technology Team of the Jet Propulsion Laboratory, Pasadena, CA, USA, during his sabbatical leave. His major research interests include millimeter-wave and terahertz devices and circuits.

Dr. Rieh was the recipient of the IBM Faculty Award in 2004, the IEEE EDS George E. Smith Award in 2002 and 2006, and the IEEE MICROWAVE AND WIRELESS COMPONENT LETTERS Tatsuo Itoh Best Paper Award in 2013. He was an Associate Editor of IEEE MICROWAVE AND WIRELESS COMPONENTS LETTERS from 2006 to 2009 and the IEEE TRANSACTIONS ON MICROWAVE THEORY AND TECHNIQUES from 2010 to 2013.